THE INSTITUTE OF ELECTRONICS,
INFORMATION AND COMMUNICATION ENGINEERS

TECHNICAL REPORT OF IEICE.

Experimental Study of Robust and High-Resolution Ultrasound Imaging Algorithm with Adaptive Smoothing Techniques

Kenshi SAHO†, Tomoki KIMURA†, Shouhei KIDERA†, Hirofumi TAKI†, Takuya SAKAMOTO†, and Toru SATO†

† Graduate School of Infomatics, Kyoto University
Sakyou-ku, Kyoto, 606–8501, Japan
E-mail: †saho@aso.cce.i.kyoto-u.ac.jp

Abstract Ultrasound imaging is an important technique with great potential for accurate nondestructive testing. Previously, we proposed a high-resolution 3-D imaging algorithm for UWB radar, the Envelope algorithm with adaptive smoothing techniques. The Envelope imaging algorithm utilizes the principle that the target boundary is expressed as an envelope of spheres determined by observed ranges, while the range smoothing techniques stabilize the estimated image produced by the Envelope algorithm by adaptively changing the range smoothing method. Numerical simulations confirm that the maximum error of this algorithm is less than 0.015 center wavelength. In this study, we apply the Envelope algorithm with adaptive smoothing techniques to high resolution 3-D acoustic imaging, which is a promising form of accurate nondestructive testing, and evaluate the performance of this algorithm with experimental data. The results verify that the proposed method achieves high-resolution 3-D acoustic imaging. The mean error of the estimated image is 6.1μm which corresponds to 8.2 $\times 10^{-3}$ center wavelength.
Key words Ultrasound imaging, high-resolution 3-D imaging, Envelope, adaptive smoothing

1. Introduction

The application of ultrasound imaging to product inspection has recently become a topic of interest. Such application, however, requires robust high-resolution imaging. Although time reversal [1] and synthetic aperture [2], [3] methods have been proposed, they are time consuming, and their resolution is insufficient.

As a solution for these problems, we proposed a high-speed imaging algorithm, SEABED, which is based on a reversible transform BST between the time delay and the target boundary [4], [5]. Although the algorithm was originally designed for Ultra Wide-Band (UWB) radar applications, it has been confirmed that SEABED can also be used to produce accurate 2-D acoustic images in high S/N cases [6]. However, this algorithm is quite sensitive to small range errors, because BST utilizes a derivative of the observed ranges.

We also proposed a fast and accurate 3-D imaging algorithm, the Envelope algorithm, for UWB radars [7]– [9]. This method calculates spheres, whose radius corresponds to the observed delay, centered at each element. This method can accurately estimate a 3-D target shape in a high S/N environment. In a low S/N case, however, the image quality of this algorithm deteriorates due to large errors on a quasi-wavefront. Here, the quasi-wavefront is defined as the relationship between sensor position and the delay of signal. To solve this problem, we proposed adaptive smoothing techniques for the Envelope algorithm [10]. These techniques were introduced for both adaptive smoothing of the quasi-wavefront and false image reduction, and realize stable imaging using the Envelope algorithm in the case of a low S/N. Numerical simulations have confirmed that the Envelope algorithm with adaptive smoothing techniques can realize high-resolution imaging in a lower S/N. The maximum error of the algorithm with smoothing techniques is less than 0.015 center wavelength with S/N $>$ 18dB. Although this algorithm was developed for UWB radar, it can theoretically be applied to 3-D acoustic imaging.

In this paper, we apply the Envelope algorithm with adaptive smoothing techniques to 3-D acoustic imaging and investigate the performance of the algorithm experimentally. The results verify that the proposed algorithm achieves high-

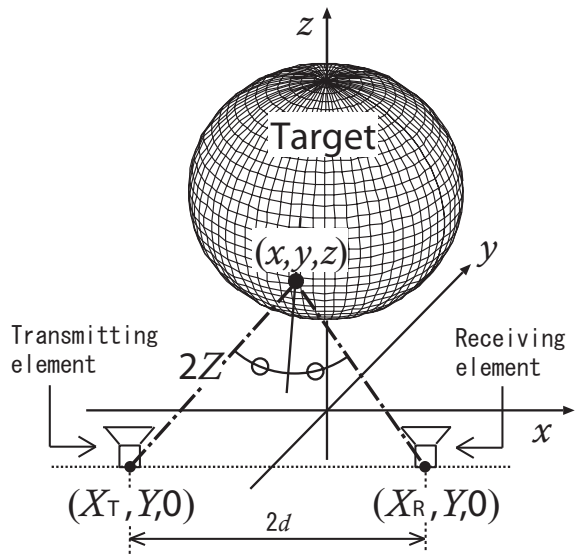

Fig. 1 System model.

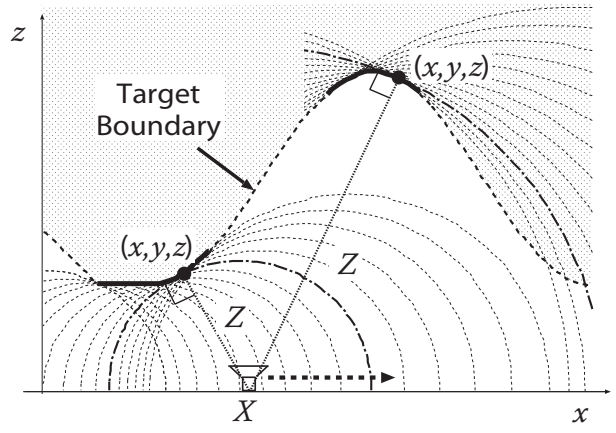

Fig. 2 Relationship between target boundary and envelopes of circles in 2-D problem.

resolution 3-D acoustic imaging in a realistic environment.

2. System Model

Fig. 1 shows the system model. It is assumed that the target has an arbitrary convex shape with a clear boundary, and that the propagation speed of the ultrasonic wave is a known constant. Transmitting and receiving elements are scanned on the plane. The separation between the transmitting and receiving elements is fixed at $2d$. We use a monocycle pulse as the voltage waveform to input into the transmitting element. R-space is defined as the real space in which the targets and sensor are located, and is denoted by (x, y, z). For simplicity, we assume $z > 0$. The locations of the transmitting and receiving elements are defined as $(x, y, z) = (X_{\mathrm{T}}, Y, 0)$ and $(X_{\mathrm{R}}, Y, 0)$, respectively. $s'(X, Y, Z')$ is defined as the received signal with the transmitting and receiving elements set to $(X_{\mathrm{T}}, Y, 0)$ and $(X_{\mathrm{R}}, Y, 0)$, respectively. Here, X is defined as $(X_{\mathrm{T}} + X_{\mathrm{R}})/2$, and $Z' = vt/(2\lambda)$ is expressed by

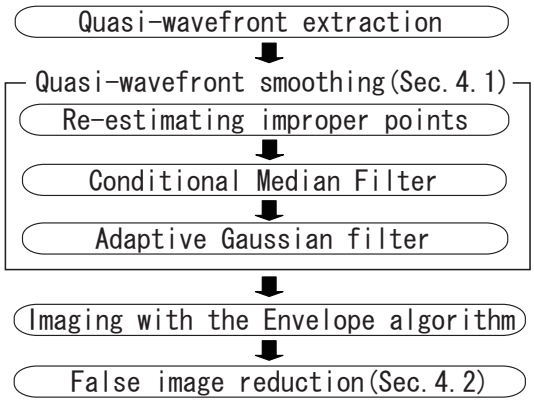

Fig. 3 The procedure of proposed imaging algorithm.

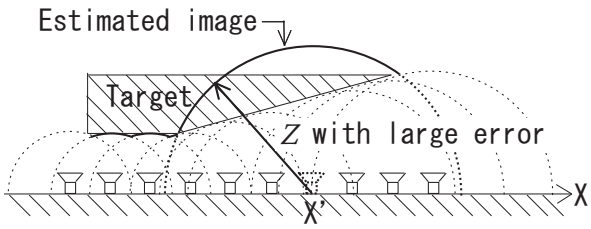

Fig. 4 The estimation example where a large error exists in 2-D problem.

the time t, the speed of the acoustic wave v, and the center wavelength of the pulse λ. $s(X, Y, Z')$ is defined as the output of the matched filter. We connect the significant peaks of $s(X, Y, Z')$ as Z for each X and Y, and extract the surface (X, Y, Z), which is called a quasi-wavefront. D-space is defined as the space expressed by (X, Y, Z). The transform from d-space to r-space corresponds to the imaging. In this paper, we utilize the Envelope algorithm for this transform.

3. The Envelope Algorithm

The Envelope imaging algorithm is based on the principle that an arbitrary target boundary can be expressed as an outer or inner envelope of spheres [7]–[9]. Fig. 2 shows the relationship between the target boundary and an envelope of circles in 2-D problems for a mono-static model. In a bi-static model, the target boundary is estimated from the envelope of ellipsoids, the focuses of which correspond to the locations of the transmitting and receiving elements. For a convex target, especially, the z coordinate of the boundary can be calculated for each (x, y) as

$$z(x,y) = \max_{(X,Y)} \sqrt{Z^2 - d^2 - (y-Y)^2 - \frac{(Z^2-d^2)(x-X)^2}{Z^2}}. \quad (1)$$

4. Adaptive Smoothing Techniques

The Envelope algorithm can realize fast high-resolution

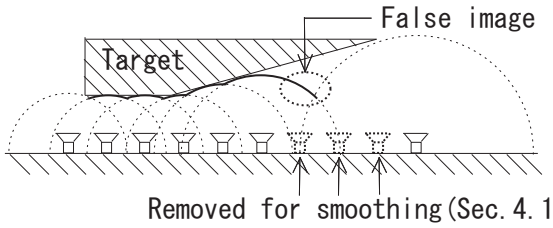

Fig. 5 The example estimated a false image in 2-D problem.

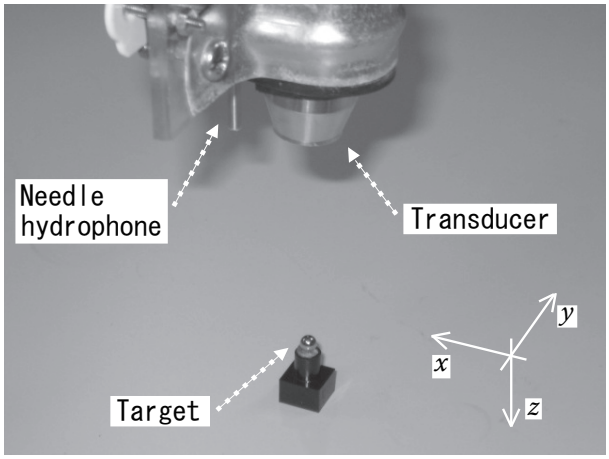

Fig. 6 Instruments utilized for acoustic imaging experiment.

imaging in an environment with a sufficiently large S/N. However, due to the large errors on the quasi-wavefront, the Envelope algorithm does not work in the case of lower S/N, because the estimated image is distorted by ellipsoids for these errors. We have proposed the image stabilization algorithm, which adaptively change the range smoothing method depending on S/N [10]. The proposed smoothing algorithm is composed of two parts:

1. Quasi-wavefront smoothing
2. False image reduction

Fig. 3 shows the procedure for our imaging algorithm. Each of the proposed smoothing methods is examined in the following subsections.

4. 1 Quasi-wavefront Smoothing

The Envelope algorithm does not obtain an accurate image where the large errors exist on the quasi-wavefront. Fig. 4 illustrates that the large errors of Z distorts the estimated image in 2-D problems. As shown in this figure, the estimated boundary in Eq. (1) is masked by a sole ellipsoid with a comparatively large radius Z. The proposed algorithm for smoothing the quasi-wavefront solves this problem by re-estimating improper points. Combined with adaptive smoothing using a Gaussian Filter and a conditional median filter it is also able to obtain more accurate range.

Here, an improper point is defined as $Z_{\rm n}$ and is estimated from noise peaks. The procedure for the re-estimating improper points is presented below.

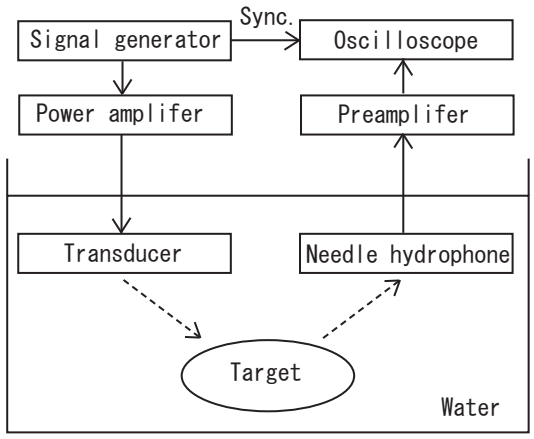

Fig. 7 Block diagram of experimental system.

Step 1). Select $Z_{\rm n}$ that satisfies $(\partial Z/\partial X)^2+(\partial Z/\partial Y)^2 > 1$ and S/N $> \alpha$. If S/N $\leqq \alpha$, we remove this point.

Step 2). Calculate for the selected point, the median value, $Z_{\mathbf{m}}$, from ranges Z of 8 adjacent elements.

Step 3). Update Z by finding the peak value of $s(X, Y, Z')$ around $Z_{\mathbf{m}} \pm \lambda$.

This re-estimating process suppresses the large errors of range. However, non-negligible errors remain on the quasi-wavefront from the re-estimation.

To suppress these errors, we utilize the conditional median filter (CMF) [11], which is suitable for smoothing a non-stationary signal, such as the quasi-wavefront. CMF calculates the median $Z_{{\rm m}i}$ from the $N \times N$ data, whose center is the input data Z_i. The output data of the CMF is calculated as

$$Z_{{\rm o}i} = \begin{cases} Z_i & (|Z_i - Z_{{\rm m}i}| < \beta) \\ Z_{{\rm m}i} & (\text{Otherwise}). \end{cases} \tag{2}$$

Moreover, to suppress the small range errors, adaptive smoothing of the quasi wavefront with a Gaussian filter has been proposed [5], where the optimum correlation length is approximated as

$$\sigma = \sqrt{\frac{\delta_{\max} Z}{\pi}}, \tag{3}$$

where $\delta_{\max}$ is the limit value of the distortion on the quasi-wavefront caused by the Gaussian filter.

4. 2 False Image Reduction Algorithm

Fig. 5 illustrates an example of estimating a false image in a 2-D mono-static problem, used for simplicity. As shown in this figure, the false image is expressed as part of the circles. To remove the false image, we have introduced an evaluation value ϕ_i. We define A_i as the area, that is estimated as part of the ellipsoids for (X_i, Y_i, Z_i). If the true shape is similar to an ellipsoid, the signal power becomes relatively large. However, if the image is incorrectly estimated as an ellipsoid, the signal power becomes small. Thus the evaluation value

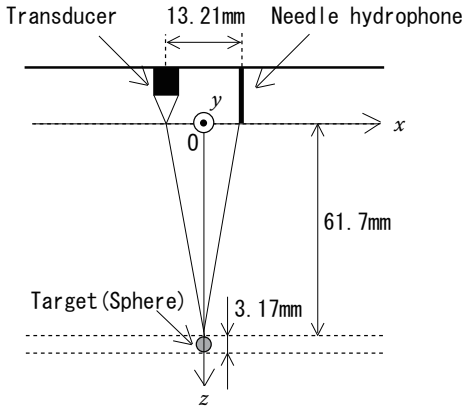

Fig. 8 Vertical section of scannning plane for the sensor and the target location.

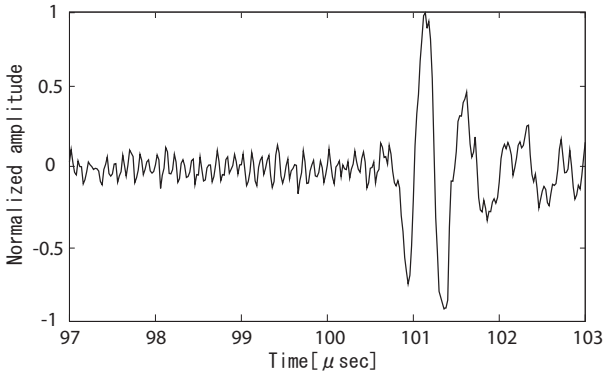

Fig. 9 Example of recieved signal.

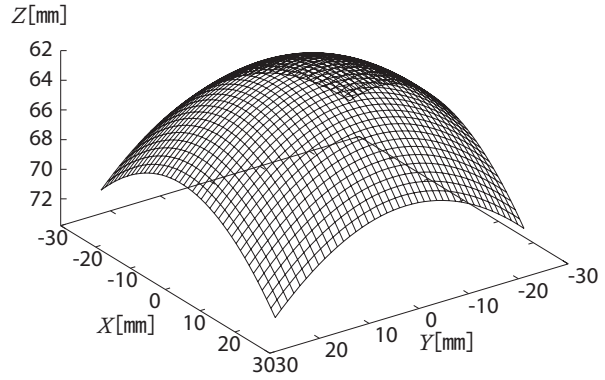

Fig. 10 True quasi-wavefront.

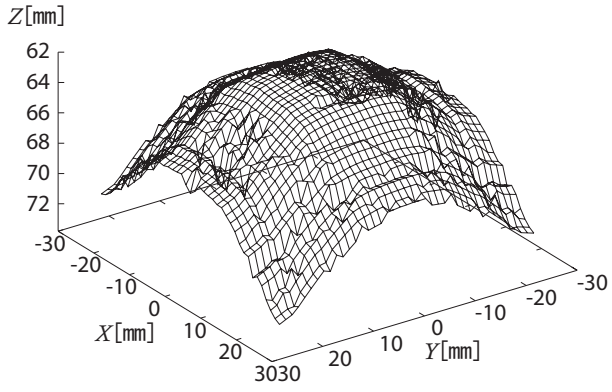

Fig. 11 Quasi-wavefront extracted from the recieved signals.

of the ith antenna location ϕ_i is defined as

$$\phi_i = \begin{cases} \max\limits_{Z'} s_i(X,Y,Z')^2/(A_i/Z) & (A_i \neq 0) \\ 0 & (A_i = 0), \end{cases} \quad (4)$$

where $s_i(X,Y,Z')$ is the received signal of the ith element location. If the evaluation value ϕ_i is small, we remove the corresponding ellipsoid.

We have already verified with numerical simulations for UWB radar that the Envelope algorithm together with these adaptive smoothing techniques can realize high-resolution imaging for a lower S/N. The maximum error of the estimated image is 0.015λ for S/N>18dB. In the next section, we apply this algorithm experimentally to 3-D acoustic imaging.

5. Experiment

5.1 Experimental Setup

Figs. 6 and 7 show respectively, a picture of the experimental setup and a schema of the experimental system. The vertical section of the scanning plane for the sensor and the target location is illustrated in Fig. 8. The separation between the transducer and needle hydrophone is 13.21mm in the y-direction. The center of the measuring unit is scanned in the range of $0 \leqq X \leqq 25$ and $0 \leqq Y \leqq 25$ mm, and the sampling interval is 1mm. A stainless sphere target 3.17 mm in diameter is put in the water, and the distance between the scanning plane and the target is 61.7mm. A transducer radiates acoustic pulses with a center frequency of 2.0 MHz and a -6dB fractional bandwidth of 0.6. Fig. 9 depicts a received signal with $(X,Y) = (0,0)$. The amplitude of the transmitted signal is amplified to 40 Vpp by a power amplifier, and then input into the transducer. The needle hydrophone receives echoes from the target, and a digital oscilloscope samples the received signals, amplified by a preamplifier. The sampled signals are coherently averaged 10000 times. The speed of the ultrasound is 1492.2m/s, calculated with water temperature of 23.5 ℃ [12], and the wavelength λ is approximately 746μm.

5.2 Imaging Results

The true quasi-wavefront and the quasi-wavefront extracted from the received signals are illustrated in Figs. 10 and 11, respectively. It can be seen that the quasi-wavefront has many large errors, especially around the side of the scanning plane. These are due to the false peak estimation of $s'(X,Y,Z')$. Fig. 12 illustrates the image estimated by ap-

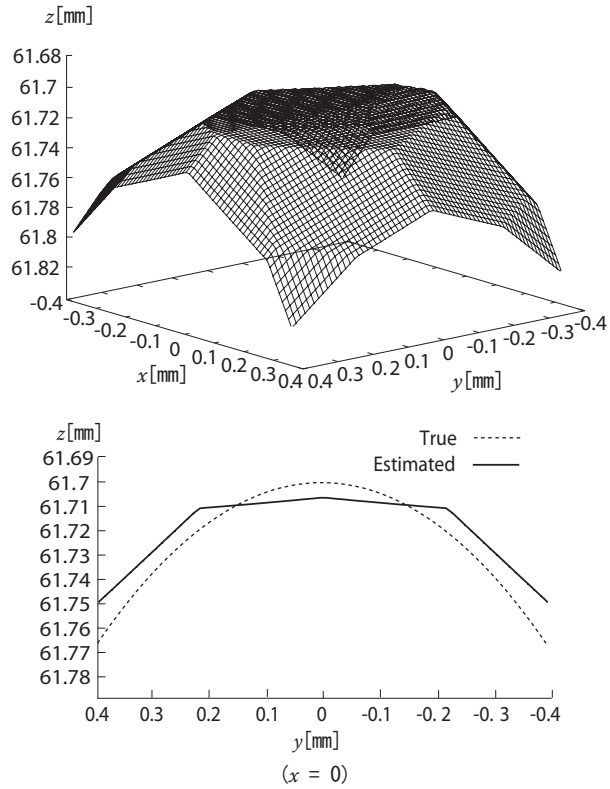

Fig. 12 Estimated image without the adaptive smoothing techniques (above) and the vertical section of the estimated image and target with x=0 (below).

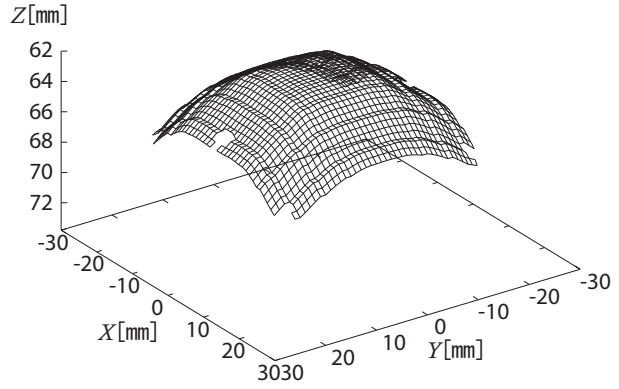

Fig. 13 Estimated quasi-wavefront with the adaptive smoothing techniques.

plying the Envelope algorithm to the quasi-wavefront shown in Fig. 11, and the vertical section of the estimated image and true target with $x = 0$. The range finding accuracy in this experiment is not sufficient to determine the location of the true target at the order of μm. Then, we translate the estimated image to the correct location by minimizing the RMS value of the difference between the true target and the estimated image. Fig. 12 shows that the estimated image is distorted by random noises on the quasi-wavefront.

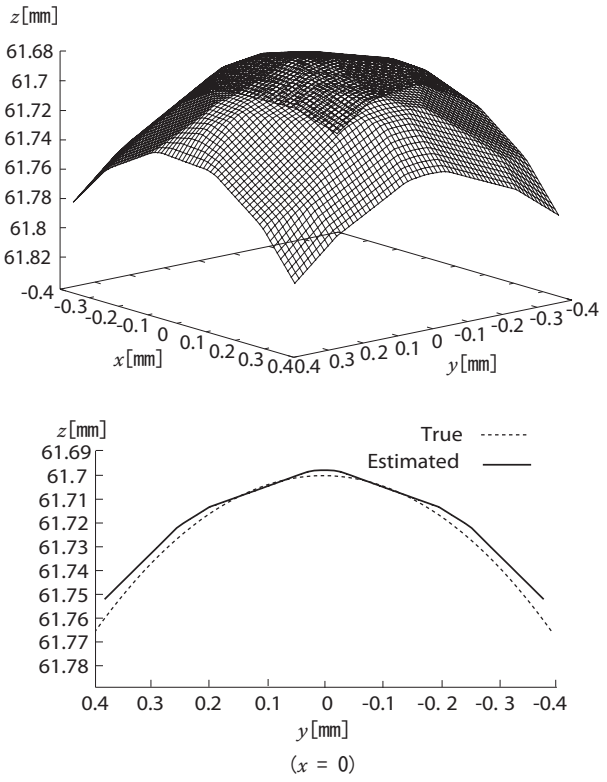

Fig. 14 Estimated image with the adaptive smoothing techniques (above) and the vertical section of the estimated image and target with x=0 (below).

Fig. 13 shows the quasi-wavefront, after applying the adaptive smoothing techniques. We empirically set $M = 2, N = 3, \alpha$=7.0dB, $\beta = 100\mu$m, and $\delta_{\max}$=90μm. This confirms that the proposed adaptive smoothing techniques can remove large errors on the quasi-wavefront. The image estimated by the proposed algorithm and the vertical section of the estimated image and target with $x = 0$ are depicted in Fig. 14, which proves that adaptive smoothing together with the Envelope algorithm realizes robust accurate imaging. The mean error is 6.1 μm which corresponds to 8.2 $\times 10^{-3}\lambda$. Moreover, the calculation time is 8.3 sec with an AMD Athlon 2.1GHz processor. This computation time is acceptable for the assumed application, which demands an imaging within 1 minute. These results indicate that the Envelope algorithm with adaptive smoothing techniques achieves high-resolution 3-D acoustic imaging, and can be used to apply nondestructive testing for product inspection.

6. Conclusion

In this paper, we have applied the Envelope algorithm with adaptive smoothing techniques to 3-D acoustic imaging, and evaluated the performance of this algorithm experimentally. The results indicate that the mean error of the estimated image is 6.1 μm which corresponds to 8.2 $\times 10^{-3}\lambda$. Moreover,

the calculation time is 8.3 sec with an AMD Athlon 2.1GHz processor. This is acceptable for the assumed applications such as product inspection. These results verify that the proposed algorithm can be applied to robust high-resolution 3-D acoustic imaging in a real environment. An important future task is to investigate the performance in the case of a complex target that includes edge and concave surfaces.

Reference

[1] S. G. Conti, P. Roux, and W. A. Kuperman, "Near-field time-reversal amplification," *The Journal of the Acoustical Society of America*, vol.121, no.6, pp.3602–3606, 2007.

[2] J. T. Ylitalo, and H. Ermert, "Ultrasound synthetic aperture imaging: monostatic approach," *IEEE Trans. Ultrasonics*, Vol.41, no.3, pp.333–339, 1994.

[3] G. P. Carroll, "The effect of sensor placement errors on cylindrical near-field acoustic holography," *The Journal of the Acoustical Society of America*, Vol.105, no.4, pp.2269–2276, 1999.

[4] T. Sakamoto, and T. Sato, "A target shape estimation algorithm for pulse radar systems based on boundary scattering transform," *IEICE Trans. Commun.*, Vol.E87-B, no.5, pp.1357–1365, 2004.

[5] T. Sakamoto, S. Kidera, T. Sato, and S. Sugino, "An experimental study on a fast 3-D imaging algorithm for UWB pulse radars," *IEICE Trans. Commun. Japanese edition*, vol.J90-B, no.1, pp.66–73, 2007 (in Japanese).

[6] T. Sakamoto, T. Kimura, H. Taki, and T. Sato, "An experimental study on a fast imaging method with reversible transform for ultrasonic short pulse," *Proceedings of the IEICE General Conference*, A–11–8, 2008 (in Japanese).

[7] S. Kidera, T. Sakamoto, and T. Sato, "A robust and fast imaging algorithm with an envelope of circles for UWB pulse radars," *IEICE Trans. Commun.*, vol.E90-B, pp.1801–1809, 2007.

[8] S. Kidera, T. Sakamoto, and T. Sato, "A robust and fast 3-D imaging algorithm without derivative operations for UWB radars, " *International URSI Commission B Electromagnetic Theory Symposium*, no.EMTS084, pp.26–28, 2007.

[9] S. Kidera, T. Sakamoto, and T. Sato, "High-resolution and fast 3-D imaging algorithm with spectrum shift for UWB pulse radars," *2nd European Conference on Antenna and Propagation (EuCAP2007)*, pp.11–16, 2007.

[10] K. Saho, S. Kidera, T. Sakamoto, and T. Sato, "Robust and high-resolution UWB pulse radar imaging algorithm with adaptive frequency compensation, " *IEICE Technical Report*, vol.108, no.30, pp.59–64, 2008 (in Japanese).

[11] T. Kasparis, M. Georgiopoulos, and E. Payne, "Nonlinear filtering techniques for narrow-band interferencerejection in direct sequence spread-spectrum systems, " *Proc. IEEE Military Communications Conference 1991*, vol.1, pp.360-364, 1991.

[12] K. V. Mackenzie, "Discussion of sea-water sound-speed determinations," *Journal of the Acoustical Society of America*, vol.70, no.3, pp.801–806f 1981.